

Numerical Investigation of the Material Behaviour during Compression Tests for Samples with Rough Surfaces Represented in Different Geometry Scale Factors

Mikhail A. Petrov^{1, a*}, Alexander N. Petrov^{2, b} and Pavel A. Petrov^{2, c}

¹Department „Machines and metal forming technologies“ & "Computer modelling and additive technologies", University of Mechanical Engineering, Bolshaya Semyonovskaya 38, 107023 Moscow, Russia

²Department „Machines and metal forming technologies“, University of Mechanical Engineering, Bolshaya Semyonovskaya 38, 107023 Moscow, Russia

^apetroffma@gmail.com, ^balexander_petr@mail.ru, ^cpetrov_p@mail.ru

Keywords: Friction Factor, Friction Coefficient, Ring Compression Test, Cylinder Compression Test, Artificial Surface Roughness, Geometry Scale Factor, Force Scale Factor, Aluminium Alloy, Titanium Alloy, Steel, FEA, QForm

Abstract. In modern technological operation, the original sample could be provided by so-called pre-operation or pre-forming follows prior the main operation. In such case, the surface roughness of the tool set is directly owned by the surface of the pre-formed workpiece, as less rigid body compared with the tool set. In metal forming practice there are mainly several pre-forming processes, among them roll forging, cross-wedge rolling and electro-upsetting. In any non-convenient forging operation route, where pre-forming is done by casting, powder sintering or any additive technology (e.g. SLS, EBM), the surface roughness and wellness obtained pre-formed workpiece could influence stronger on the quality of the end part after main forging operation. In order to investigate the different materials' behaviours depends on the surface artificial roughness the finite-element analysis (FEA) was carried out for the simple compression tests, thereby the cylindrical, made from aluminium and titanium alloys, and ring specimens, made from steel, were compressed between two flat dies with modelled zero and non-zero roughness at room and elevated temperatures. The behaviour of the lubricant (fluid phase) positioned between two neighbored peaks of the roughed surface was investigated in one direction material flow test as well. The results have shown the strong pressure increase in the bottom area of the peaks, which correspond the practice case, when the fluid phase is not completely evaporated after lubrication. Further, it can course the different microstructure evolution during hot forging operation and during cold bulk forming operation, additional surface pressure can result the material hardening near to the contact zone (not investigated here). In commonly, in observed results the peaks of the roughness can be easily broken due to enormous tangential stresses, as it is well known from the fundamental investigations. Moreover, the computation of geometry scaled tools and workpieces of the ring compression and one-direction material flow tests resulted the exponential dependency against the deformation forces.

Introduction

Depends on the localisation of the friction the geometry of the workpiece changes differently. From another point of view, the friction interpretation is conducted with the contact pressure. In the simplest way the pressure is the ratio of the force to the summarized contact area for the ideal surface, i.e. the surface does not have waviness and roughness. Assuming the fact that each surface quality is directly dependents from the processing method the summarized pressure should be predicted as the ratio of the sums of acting forces ($\sum_{i=1}^q F_i$) to the area ($\sum_{j=1}^m s_j$), which is concentrated between two neighbored peaks or valleys on a certain length (Eq. 1).

$$P = \sum_{k=1}^n \left(\frac{\sum_{i=1}^q F_i}{\sum_{j=1}^m s_j} \right)_k \quad (1)$$

There are five main types of the surface nonlinearities (Fig. 1). To them belong macroroughness, waviness, roughness, micro- or subroughness and nanoroughness (not shown). Nanoroughness is rather new for fundamental understanding topic, which operates with the dimensions equivalent to atomic size. It is well-known, that the surface quality depends on the processing technologies. For milling and turning, the asperities arrange and build up a periodic profile. Contrary the grinding and eroding operations provide an aperiodic profile. During any forging operation the periodic profile of the initial blank changes to aperiodic.

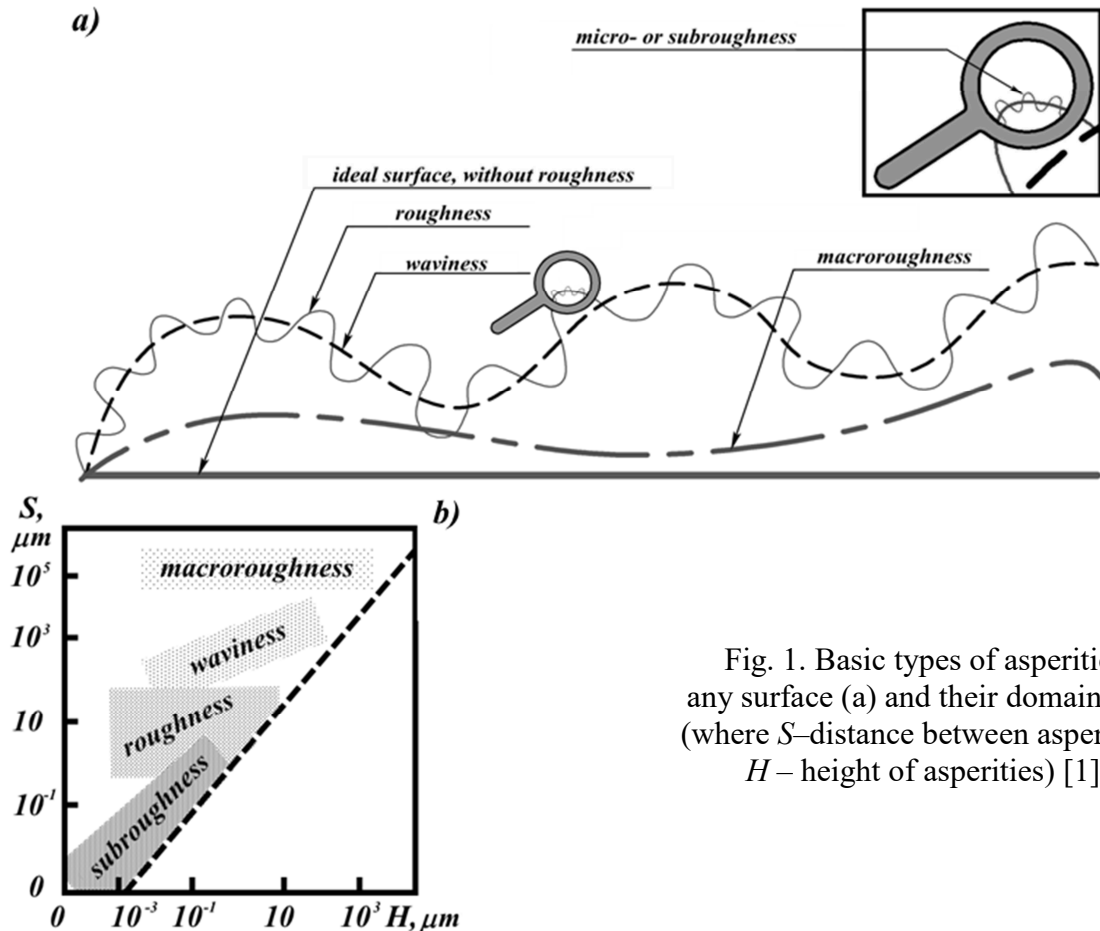


Fig. 1. Basic types of asperities of any surface (a) and their domains (b) (where S —distance between asperities, H —height of asperities) [1]

The roughness can be easily measured with the help of standard devices working on inductive contact principle (up to microroughness), of micro-computer tomography (MCT) or of the atomic force microscopes, which are acting on the attractive and repulsive forces of the atoms (up to nanoroughness) [2, 3]. As a rule the output of such devices, presents the 2D linear roughness or 3D topography map. Its integration into the computer aiding engineering software is the task of the future digitalisation of the production facilities to improve the product quality. Even the obtained successful result will demand the strategy of the further computer calculations of the roughness in respect to the permanent geometry changing and interaction of the peaks and valleys. This task is quite similar to the simulation of the microstructure evolution.

It is proposed, that the curve depicted the deformation force distribution depends on the surface roughness has non-uniform behaviour. Physically, the initial point (F_0) and force is directly depended on the roughness (Fig. 2), whereby there is an average meaning of roughness (curve R1). Actually, there is no zero-equal point for the beginning of each of the curves. The reason is that the asperities of the rough surface contact the punch and the force should be applied to deform it prior the main curve's growth occurs due to the volume deformation. So the force F_0 has minor value and lay quite near to zero. Close to the punch displacement corresponded S_1 the force riches the certain value (F_1) as a result of the roughness changes. Now the specimen reproduce the roughness of the more rigid body – the tool set. Theoretically, after that point the force curve does not have a roughness-related term inside. It means that the roughness could be neglected. Such an approach is

more simplified in the technology-oriented FE-codes. During the numerical simulation the roughness is neglected from the beginning and the pressure distributes on the complete side surface uniformly (curves R1, R2 and R3). It means that the zero point and the F_1 are connected by simple linear function. Therefore, the force-displacement curve (RNS) have to begin not from zero point but from F_0 (Fig. 2). The area of the contact surface and consequently the force increase constantly during the deformation, whereby the pressure decrease due to the well-known equation. The duration of the gap with non-uniform force changing and so the slope of the curve depends on the surface roughness.

Following methods are practically used to estimate the friction related parameters: cylinder upsetting test (CUT), ring compression test (RCT), cup or double extrusion (DCET), forward-backward extrusion (FBET), T-shape extrusion test (TSET), one-direction material flow test (ODMFT) also known as extrusion in narrow channel (ENC) etc. Each of the methods has its' limits due to the contact pressures on the tools' contact surface [4] and stress-strain materials' characteristics. Indirectly friction can be assessed on the material flow behaviour. For several tests, e.g. RCT and TSET, there is a neutral layer (NL) to be pointed out [5] (Fig. 3). The NL divides the opposite oriented velocity vectors of material flow and its location depends on the contact pressure and friction conditions. Has the material intensive flow in radial direction, so lay the NL for RCT outside the sample. The contribution of the surface roughness into material behaviour is weakly developed for these tests. Many efforts were done to understand the role of the surface roughness in metal forming processes [6, 7]. Jeng in [8] used the simple linear roughness measurements (2D, ISO 4287) of the specimen subjected to the experiments on the pin-on-disc tribometer. He found out that the lower roughness is, the lower is the friction. Moreover, the friction for roughness in longitudinal direction is higher than for transverse roughness. Doege et al. showed elsewhere [9] that the using of fractal model is mathematically more advantageously and simple then the reconstruction of the obtained by linear roughness measurements profiles in case of sheet metal forming. Hisakado presented in [10] the conical asperity model to investigate the deformations between the rough and flat surfaces. He had also investigated the contact problem for different radii of curvature of asperity peaks [11]. Sutcliffe in [12] investigated the crash of the asperities under bulk deformation of the underlying material in longitudinal and transversal directions based on the energy method.

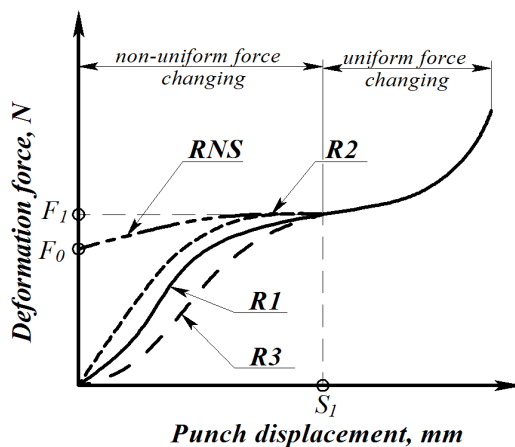


Fig. 2. Expected force – punch displacement curves for three arbitrary initial roughness values of the surface (R1, R2 and R3)

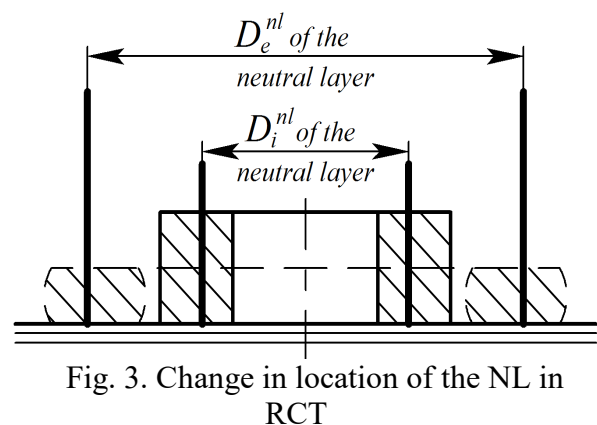


Fig. 3. Change in location of the NL in RCT

With the time, the information on linear roughness was expanded on the area (ISO 25178) to obtain 3D-pictures of surface topography. Stahlmann et al. used an own approach based on the calculation of the root mean square height (S_q) to estimate the surface evolution during the extrusion [13]. Leu in [14] took into account the strain-stress characteristics of the asperities on the contact surface during compression and purposed another approach. Menezes et al. in [15] discussed the pin-on-plate tribological test and concluded that the friction coefficient was controlled by the surface topography and not the surface roughness: the plowing and adhesive components and stick-

slip phenomenon depended in a strong manner from it. The macroscopic deterministic surface structures were prepared and investigated by Groche et al. in [16]. It was shown that the friction on microscopically structured specimen subjected to cold deformation in slide-compression test could be reduced on up to 40% compared to the blasted reference specimens. In addition, the lubrication of the specimen before forward cold extrusion provided the changes of surface topography [17, 18].

Chiang et al. investigated the dynamic friction properties of the samples made from extruded magnesium alloy AZ31 applying the RCT at elevated temperatures [19]. They found out, that even the surface quality (machined with $R_a = 0,15 \mu\text{m}$ vs. polished with $R_a = 0,09 \mu\text{m}$ specimens) played a little role on the changing of the friction coefficient. Jung et al. in [20] investigated the friction during the deformation of the aluminium cylindrical specimen under room temperature at different deformation speeds and lubricants using the pin test. The evolution of the punch roughness was recognized on the surface topography captures. From the analysis of the obtained loading curves they concluded that the lubricant's type plays an important role, because due to the changing tools' surface topography the location of the lubrication pockets also changes and the hydrodynamic effect results the increase in deformation force. Hubert et al. had developed a FE-model, which had taken surface roughness, drawing force and lubricant's layer thickness in account, shown elsewhere [21]. During strip drawing the significant influence was executed by the drawing speed, so at higher speed values the greater amount of the lubricant escaped from the pockets on the contact surface than at lower speeds. Carretta et al. applied an own numerical FE-model regarding the asperity geometry successful for cold rolling process [22]. Karpenko & Akay did numerical computation of the friction force for two contacted rough plates in [23].

Eriksen et al. investigated three surface qualities applied to microforming area of metal forming [24]. As expected, the results were not straightforward. During the double cup extrusion test of α -copper alloy CuZn15 performed in the dies of $\varnothing 1 \text{ mm}$ and $\varnothing 2 \text{ mm}$ with different roughness for lubricated specimen the friction factors (FF) changes. For the die of $\varnothing 1 \text{ mm}$, the lower values of FF corresponded more rough specimens and for the die of $\varnothing 2 \text{ mm}$, the same dependence was inverted.

Simulation procedure

Roughness design and numerical simulation. To simulate the behaviour of the non-ideal surface the roughness of the initial geometry was generated according to the Eq. 2 (further designated in form of AxFx.xxx). The coefficients of the equation and its correspondent 3D-models are presented in the Table 1. The macroroughness and waviness were neglected.

$$y = A \sin\left(\frac{x}{F}\right), \quad (2)$$

where roughness coefficient A – represents the amplitude change of the asperity; roughness coefficient F – represents the period of the asperity.

The profiles of the asperities were generated in MS Excel[®] and the 3D-models were created in T-Flex[®]. The first software uses the Bezier curves; meanwhile the second software uses non-uniform rational B-spline (NURBS). The results looks similar but at certain magnification the geometry of the peaks of the curves are not fine and uniform any more (Fig. 4). Contrary the peaks are staying fine and smooth in 3D-model. That let us assume, that the description of the asperities is not a trivial task. Therefore, in this article the profiles based on the NURBS-curves (CAD-software) were under study.

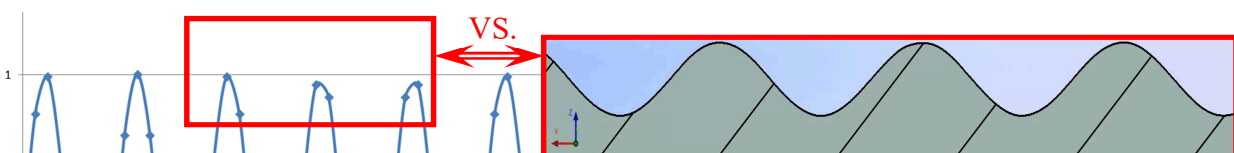

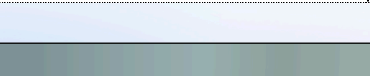


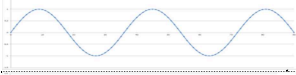

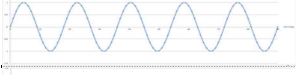
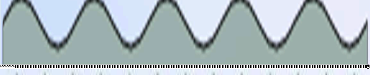

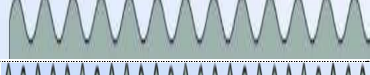
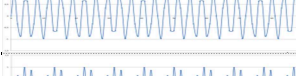
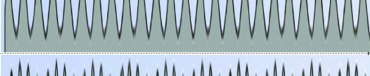
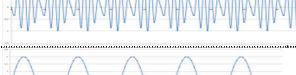
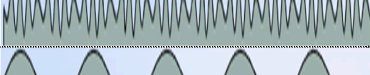
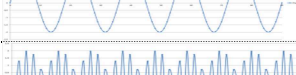
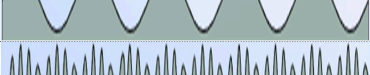




Fig. 4. Roughness description for $A=1$ and $F=0,02$ by: Bezier-curves (left) and NURBS-curves (right)

Simulations were performed for four different materials to understand various effects using the FE-code QForm[®]. The mechanical properties of the investigated materials are given in the Table 2. The conclusions to the obtained results were carried out on four main investigations: simulation of non-constant friction distribution in RCT and simulations of roughness related tests (CUT, RCT and ODMFT). Due to the fact, that the QForm is a software for calculation the technological processes, many physical aspects of the process are neglected or simplified, e.g. diffusion, heat radiation, tools' wear, friction etc. Due to the size difference between roughness (measured in μm) and tools' dimensions (measured in mm) the simulated roughness was scaled up to 1000 times to perform the triangulation of the geometry and create the FE-mesh correctly. Such approach simplified the task, at the same time reduce the calculation time and required machine capacity as well.

Table 1. Investigated surface profiles

Formula & Designation	Coefficients' means		Curve of the function	3D-model of artificial roughness (asperities)	FE-mesh*
	A	F			
$y = 0$ A0F1	0	1			TSP
$y = \sin(x)$ A1F1	1	1			n/s
$y = \sin(10x)$ A1F0,1	1	0,1			TSP
$y = \sin(20x)$ A1F0,05	1	0,05			TSP
$y = \sin(50x)$ A1F0,02	1	0,02			TSP
$y = \sin(100x)$ A1F0,01	1	0,01			TSP
$y = \sin(200x)$ A1F0,005	1	0,005			TNP
$y = 2\sin(20x)$ A2F0,05	2	0,05			TSP
$y = 2\sin(200x)$ A2F0,005	2	0,005			TNP

*TSP – triangulation successful proceeded; TNP – triangulation not proceeded; n/s – not simulated

According to the information, given in [250], it is based on flow formulation, where the independent variables are velocity vector and mean stress. In rigid-visco-plastic model the material is considered as incompressible, isotropic continuum and elastic deformations are neglected. The constitutive equation (Eq. 3) is used to describe the material flow. The effective stress depends on the effective strain ε , the effective strain-rate $\dot{\varepsilon}$ and temperature T. The value of middle stress (σ_m) is being calculated as a one-third from the sum of the normal stress components of the stress tensor, placed on the major diagonal in stress matrix (Eq. 4).

$$\sigma_{ij} = 2/3 \left(\bar{\sigma} \dot{\varepsilon}^{-1} \dot{\varepsilon}_{ij} \right), \quad (3)$$

$$\sigma_m = 1/3 (\sigma_{11} + \sigma_{22} + \sigma_{33}), \quad (4)$$

where σ_{ij} – the stress tensor components, $\bar{\sigma}$ – the effective stress (flow stress), $\dot{\varepsilon}$ – the effective strain-rate, $\dot{\varepsilon}_{ij}$ – the strain-rate tensor components, σ_{11} , σ_{22} and σ_{33} – normal stresses.

As a friction model the Levanov's friction model was applied (Eq. 5), for which the fundamental description can be found elsewhere [25, 26].

$$\tau = m \frac{\sigma_{cs}}{\sqrt{3}} \left(1 - e^{\left(-n \frac{\sigma_n}{\sigma_{cs}} \right)} \right) \quad (5)$$

$$\mu \approx \frac{m}{\sqrt{3}}, \quad (6)$$

where m – friction factor; μ - friction coefficient, n – Levanov's coefficient, ($n = \text{const} = 1,25$); σ_n – normal contact pressure in given point of contact surface, [MPa]; σ_{cs} – yield stress of layer in workpiece near contact surface with die, [MPa].

The virtual work-rate principle and finite element technique are used to obtain the non-linear system of algebraic equations describing the material forming process. The system includes such equations as equilibrium equation, compatibility equation, constitutive equation as (Eq. 3) and incompressibility. Energy balance equation is treated by means of the weighted residual method (Galerkin's method) resulting in a system of ordinary differential equations that is integrated numerically. The indexes i and j for two-dimensional problems vary from 1 to 2. Velocity and mean stress fields are approximated by quadratic and linear shape functions, respectively, within the 6-node triangular elements with curved sides. The finite-element mesh is generated automatically. During simulation, the decrease of the mesh density for small material volumes occurs also automatically through a special remeshing algorithm of the program.

The desktop configuration was as follow: Intel Core i7 – 2600 CPU 3.4 GHz with 8 processors, 64-bit, 8 GB RAM and NVidia GeForce GTX 670 with 2 GB RAM. All simulations were done according to the map presented in the Fig. 5.

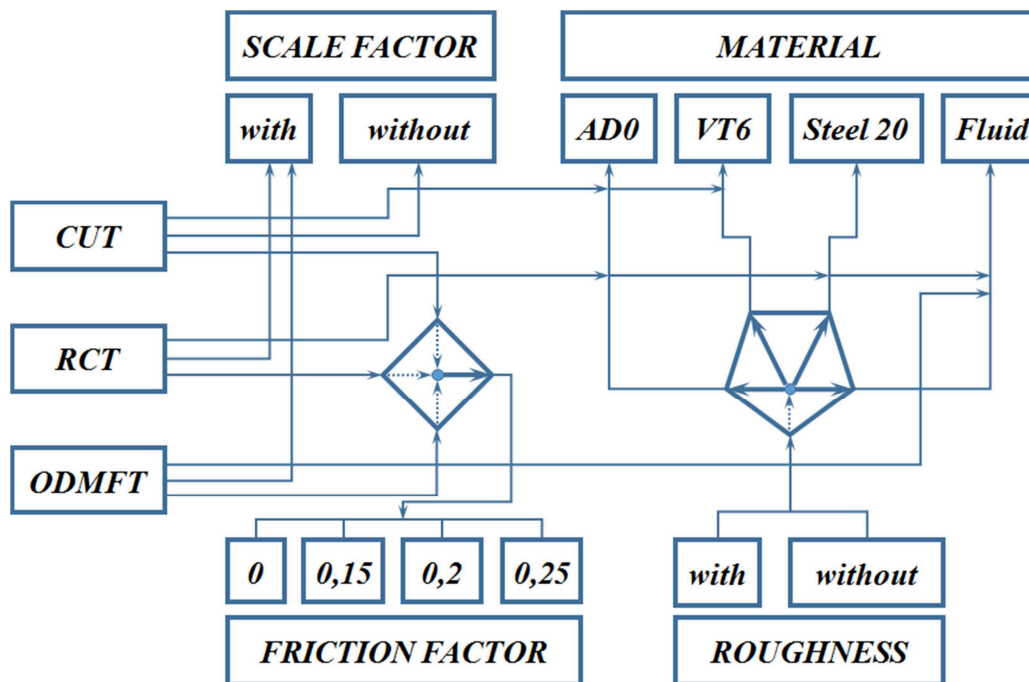


Fig. 5. Map of the numerical simulations

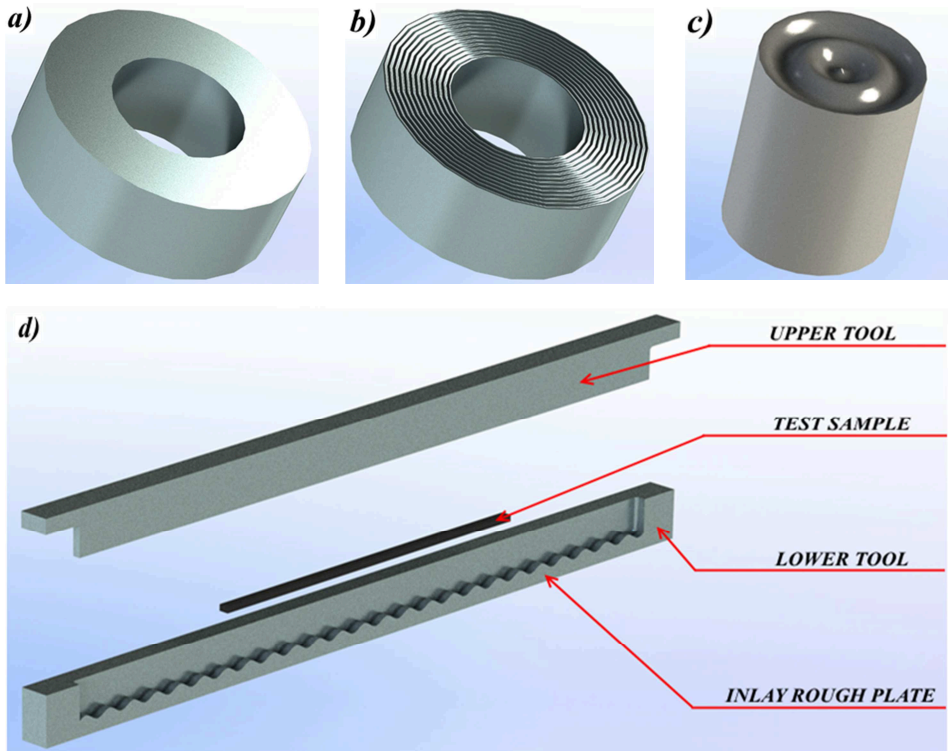


Fig. 6. 3D-models of the ring steel samples with ideal surface (a), with rough surface and $A=1$, $F = 0,02$ (b), cylinder aluminium specimen with $A=1$, $F = 0,02$ (c) and tool set with narrow channel for one way material flow, in longitudinal direction (d) (photorealistic representation, designed in T-Flex CAD[®])

Table 2. Mechanical properties of the materials

Parameter	Value	Parameter	Value
Aluminium alloy AD0* (solid phase)		Steel 20 (solid phase)	
Yield stress, [MPa]	function of $\dot{\epsilon}$, T and ϵ	Yield stress, [MPa]	function of $\dot{\epsilon}$, T and ϵ
Density, [kg/m ³]	2 710	Density, [kg/m ³]	7 833
Thermal capacity, [J/kgK]	930	Thermal capacity, [J/kgK]	494
Thermal conductivity, [W/mK]	226	Thermal conductivity, [W/mK]	52
E-module, [GPa]	75	E-module, [GPa]	213
Poisson ratio	0,33	Poisson ratio	0,3
Lubricant-like material(fluid phase)		Titanium alloy VT-6* (solid phase)	
Yield stress, [MPa]	0,1	Yield stress, [MPa]	function of $\dot{\epsilon}$, T and ϵ
Density, [kg/m ³]	1 080	Density, [kg/m ³]	4510
Thermal capacity, [J/kgK]	1 800	Thermal capacity, [J/kgK]	930
Thermal conductivity, [W/mK]	0,12	Thermal conductivity, [W/mK]	17,4
E-module, [GPa]	4	E-module, [GPa]	115
Poisson ratio	0,4	Poisson ratio	0,32

* For AD0 the European analogue is EN AW-1050 and for VT-6 \rightarrow Ti-6Al-4V

To the solid phase materials belong steel, aluminium and titanium alloy. The lubricant-like material (fluid-phase) is the equivalent to the real used lubricant's material with the properties neared to the viscous Newtonian liquid. Meanwhile its precise physical properties were not determined and applied here.

Non-constant friction (ideal contact surface). The ring samples with the standard rounded in case of diameters ratio of 6:3:2 (multiplier 7), that means the dimension of outer diameter $D = 40$ mm, inner diameter $d = 20$ mm and height $H = 14$ mm, were subjected to the compression test (Fig. 6a). Meanwhile the friction conditions were different. There were four cases under study, namely without friction (case A), with high friction ($FF = 0,35$) in a quarter segment of the ring (case B),

with high friction ($FF = 0,35$) in the centre and low friction ($FF = 0,15$) in the peripheral zone (case C) and at last with frictionless centre zone and high friction ($FF = 0,35$) in the peripheral zone. The FF -values corresponded the values obtained from the experimental results of the previous studies for aluminium alloys [27, 28]. The results were used as a certain reference, which provided the possible disturbance of the geometrical volume during deformation.

Roughness influence (in cylinder upsetting test – CUT). The cylinder specimens with the height of $H = 30$ mm and diameter of $\varnothing 25$ mm were used (Fig. 6c). The roughness profile according to the Table 1 was applied on the workpiece contact surface with the punch only. Aluminium and titanium alloys were under study. Deformation of the Ti-alloy was performed at elevated temperatures under isothermal conditions ($T = 750^{\circ}\text{C}$). The scaling dependence output was not requested here. The relationships between deformation force (F) and designed roughness have to be determined.

Roughness influence (in RCT). 3D-models of the ring specimens have one rough side surface in compliance with the Table 1 and Fig. 6b. The compression occurs between two flat plates. Additionally the rings were compressed in four scale modifications of geometry: M1:1, M5:1, M10:1 and M15:1. Based on it the influence of the roughness and both geometry and force scale factors have to be defined. Steel 20 was under study. Also the behaviour of the lubricant-like material was under study here.

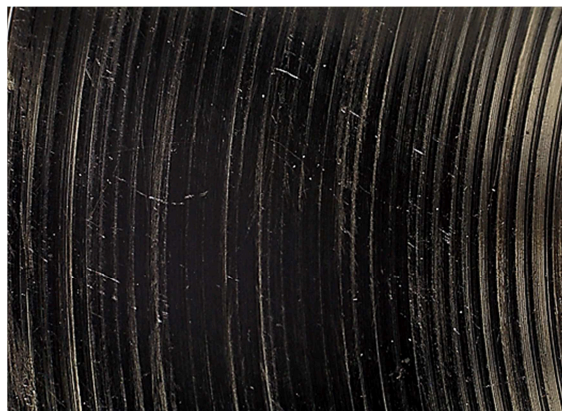
Roughness influence (in ODMFT). Lubricant-like material with the properties from the Table 2, the thickness of 2, 6 and 10 mm and common length of 90 mm was compressed between the rough inlay plate and the upper tool (punch) according to the tool's construction in the Fig. 6d. The relationships between deformation force (F) and lubricant thickness-designed roughness have to be determined.

Experimental procedure

The evaluating procedure to the dependence force – punch displacement (Fig. 2) was carried out on the experimental results, which include the data from the ring compression test for steel 20. Two types of surface quality have been chosen.

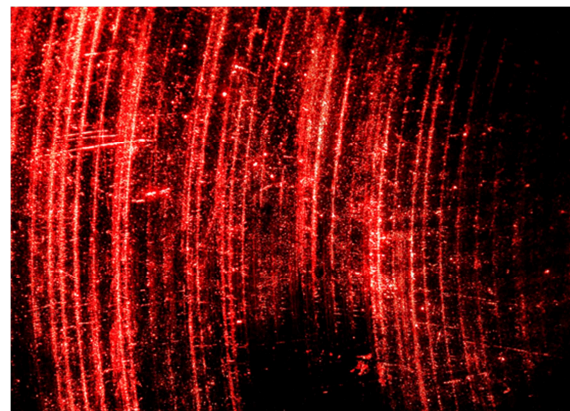


a)



b)

Fig. 7. Standard ring samples for RCT (a); microscopic captures (USB-microscope, max. magnification up to $\times 300$): one of the side surfaces of the ring specimen (b) and its representation in laser reflected beam (c)



c)

Ring compression test (RCT). The test was performed on the mechanical crank press of 1,6 MN applying ring samples with grinding (low roughness) and turning (high roughness) side surfaces. The average tools' temperature was 140 – 150°C. There were two water-based arts of the lubricant under study: with thermo- and natural graphite. The dilution of the lubricants was 1 to 10. The lubricant was sprayed on the punch and die surface through the nozzle system of $\varnothing 3$ mm within 2,5 seconds that had guaranteed the base evaporation before the process begin. The ring samples have the standard ratio of 6:3:2 (Fig. 7a). The relief of the turned surface is typical for this kind of machining and can be recognized on the bright and dark circles (Fig. 7b). It is also good to see in reflexion of the laser beam: the bright circles represent the peaks and the dark – the valleys of the asperities (Fig. 7c). Friction coefficients were found as a function of the inner diameter and tool's temperature. The technique was described in earlier publications elsewhere [29, 30, 31]. Eq. 6 explains its dependence from the friction factor.

Results and discussion

Simulation: non-constant friction (in CUT and RCT). Firstly, the geometry distortions of the ring samples were stated (Fig.8a). In case A the weak barrel-like form with near to infinity curvature of the free surface and small radii on the edges occurred.

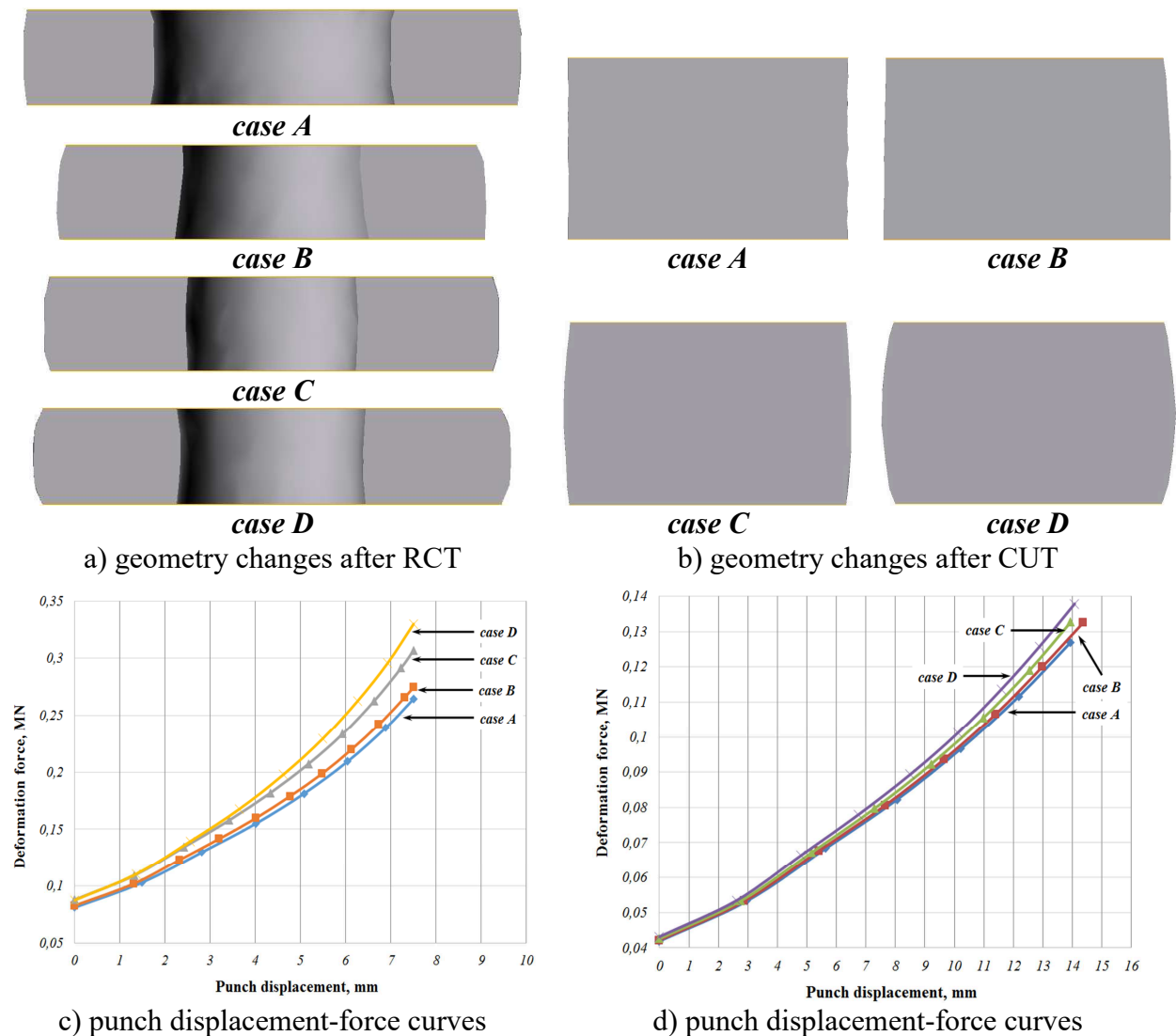


Fig. 8. Material flow at the end of RCT (a) and CUT(b) for AD0 with $m = \text{var}$ (case A – barrel-like or barrel-free form; case B – distorted barrel-like form; case C – double convex- or barrel-like form; case D – barrel-like form) and corresponding loading curves (c, d)

The maximal outer diameter and very intensive material flow in transversal direction were observed. If the friction concentrated on the quarter of the ring surface (case B) the geometry was divided in horizontal plane into two regions, i.e. with and without curvature, which prevent the material flow in transversal direction in a strong manner. In the third case (case C), the material flows more intensive in radial direction as in case B due to the symmetrically applied friction in the central part. At last, combination of the strong and weak friction provided the intensive material flow from the centre and deferred in the peripheral part (case D). In case A of the cylinder workpiece (Fig. 8b) the frictionless material flow in radial direction resulted the geometry with infinity curvature, i.e. the linear free surface. The result for case B is the combination of the friction free and friction problem formulations, i.e. the linear and light barrel-like forms occurs. The strong friction on the contact surfaces of the case C and D result the pure barrel-like forms. In case D the summarized per area friction is higher as in case C, so the free surface curvature is lower for case D. Comparing the corresponding cases for RCT and CUT following can be concluded, that the geometry of the free surface has more modification possibilities in case of RCT comparing with the CUT. It confirms the well-known fact, that the RCT is more sensible to the changing of the friction conditions. Also from the graphical point of view, the distances between the curves corresponded the investigated cases are bigger for the RCT than for the CUT (Fig. 8c vs. 8d).

Simulation: roughness influence (in RCT). On the fifth, calculation step the height decrease of the asperities could be recognized. During the compression stage, the asperities were completely smoothing down on the eighth step (Fig. 9).

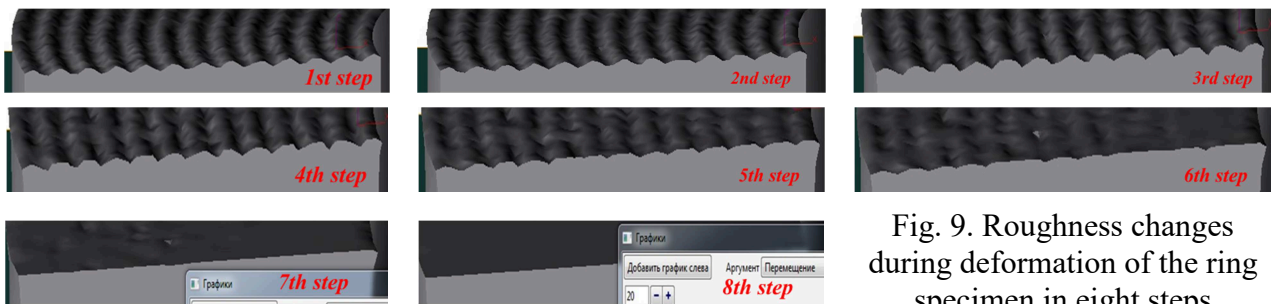


Fig. 9. Roughness changes during deformation of the ring specimen in eight steps

Table 3. Force values for steps from the Fig. 9

Step number	1	2	3	4	5	6	7	8
Punch displacement, [mm]	0	0,19	0,52	0,77	4,15	8,69	18,08	27,62
Deformation force, [MN]	17,8	30,3	47,1	45,9	47,9	51,5	62,4	74,8

Increased contact area of the deformed peaks increases the deformation force (step 1 vs. step 6) and reduces the contact pressure for dry friction case as expected (Fig. 9 and Table 3). The number of the finite elements at the end of calculation differs from the beginning stage. For example, for the roughness with coefficients $A = 1$ and $F = 0,02$ at scale M10:1 the number of volume elements reached the number of 140 528 before vs. 20 434 after calculation. Therefore, the small drop down of the force (Table 3 and Fig. 9, 10) was observed on the fourth step and can be explained by remeshing procedure and achieving the yield stress values by the peaks.

The presented reference curves for four geometry scale factors and free of roughness surfaces (Fig. 10a) coincide with the obtained force-displacement curves for rough surfaces. It means that after the fourth step the force was quit independent from the roughness coefficients (Fig. 10b, c). Nevertheless, closer look at the non-uniform force changing area reveal the deviations of the curves for rough surfaces from the curves for ideal surfaces. Their waveforms with different periods represent the continuous increase of the contact area and consequently the deformation force (Fig. 10d). Due to non-symmetrical placing of the ring lubricant's specimen, the NL located not symmetrical to the CL. In addition, material has preferred flow direction due to not equal ring contact areas and summarized friction forces on the left and right side from the CL at the end of

calculation. In addition, velocities (Fig. 11a) and plastic deformations (Fig. 11b) were not symmetrical. During material propagation in radial directions, the located in peaks at the process beginning the deformation zones migrated downwards except the located near to or on the CL.

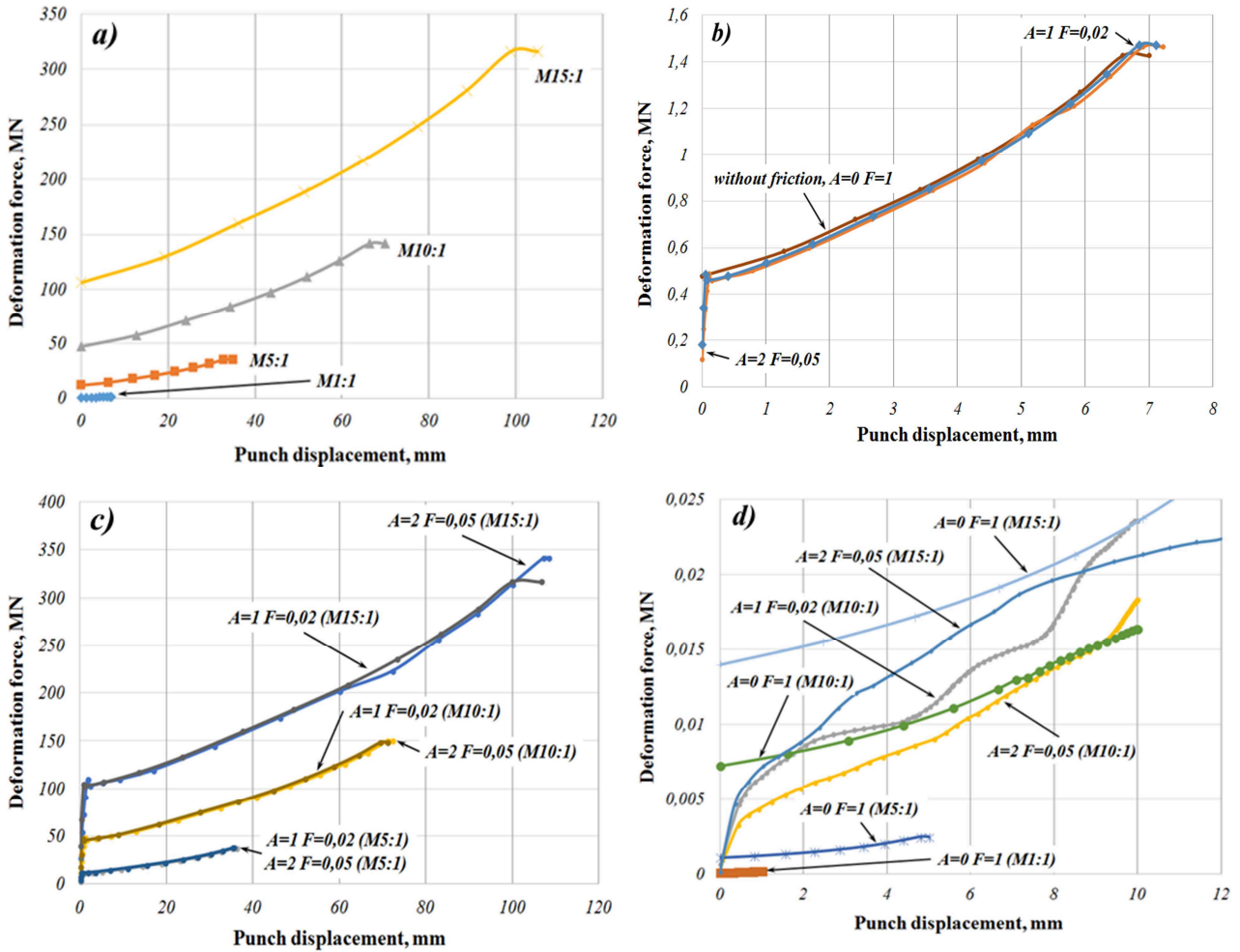
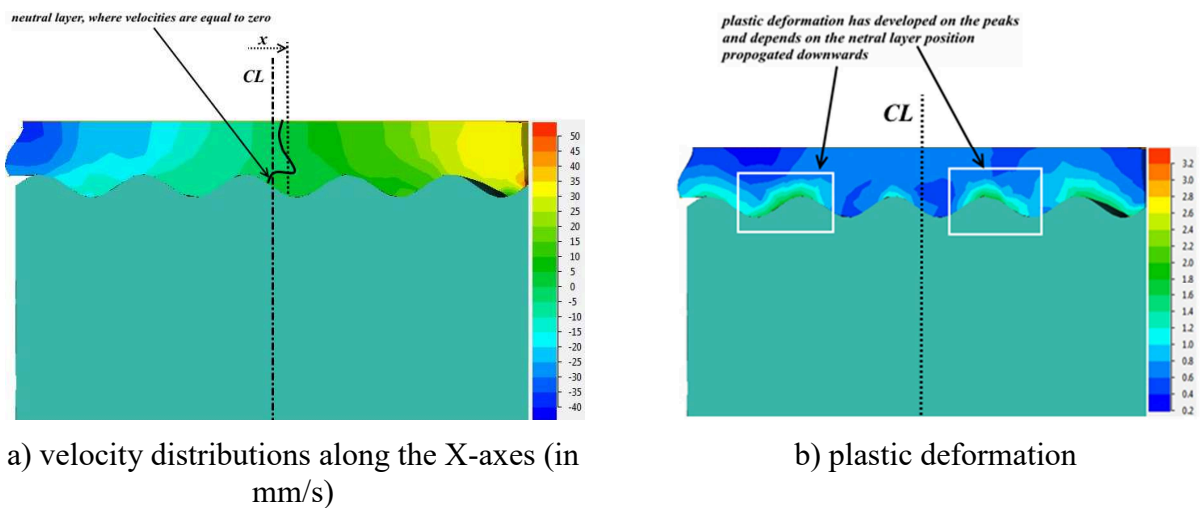


Fig. 10. Punch displacement – deformation force curves for steel 20 for: the ring specimens with $A = 0 F = 1$ (zero roughness, ideal surface) and four scales (M1:1, M5:1, M10:1, M15:1) (a), with different surface roughness and scale M1:1 (b), with different surface roughness and scales (M5:1, M10:1, M15:1) (c); the ring lubricant volume compressed on the rough die (d)



a) velocity distributions along the X-axes (in mm/s)

b) plastic deformation

Fig. 11. Displacement of the NL from the centreline (CL) (a) and evolution of the deformation areas (b) on the 56th simulation step for A2F0,05 and scale M10:1

Simulation: roughness influence (in CUT). As it was stated, the CUT is less sensible as RCT. As a result, the obtained curves do not provide any useful information to the influence of the FF (Fig. 12). However, the more expressed gaps between the curves for Ti-alloy and their order comparing to the corresponding cases for Al-alloy indicate their dependence from the roughness coefficients. The lowest derivations up to 3% of the curves' set for three FF were in the middle of the curves. The highest derivations up to 7% were observed at the beginning and at the end of several curves within the domain, which correspond the calculation error for FEA. Moreover, in the Fig. 12b the contribution of the lubricant-like material calculated for ideal surface is given. For the rough surface, the appropriate curve will take place under it so the force will be less.

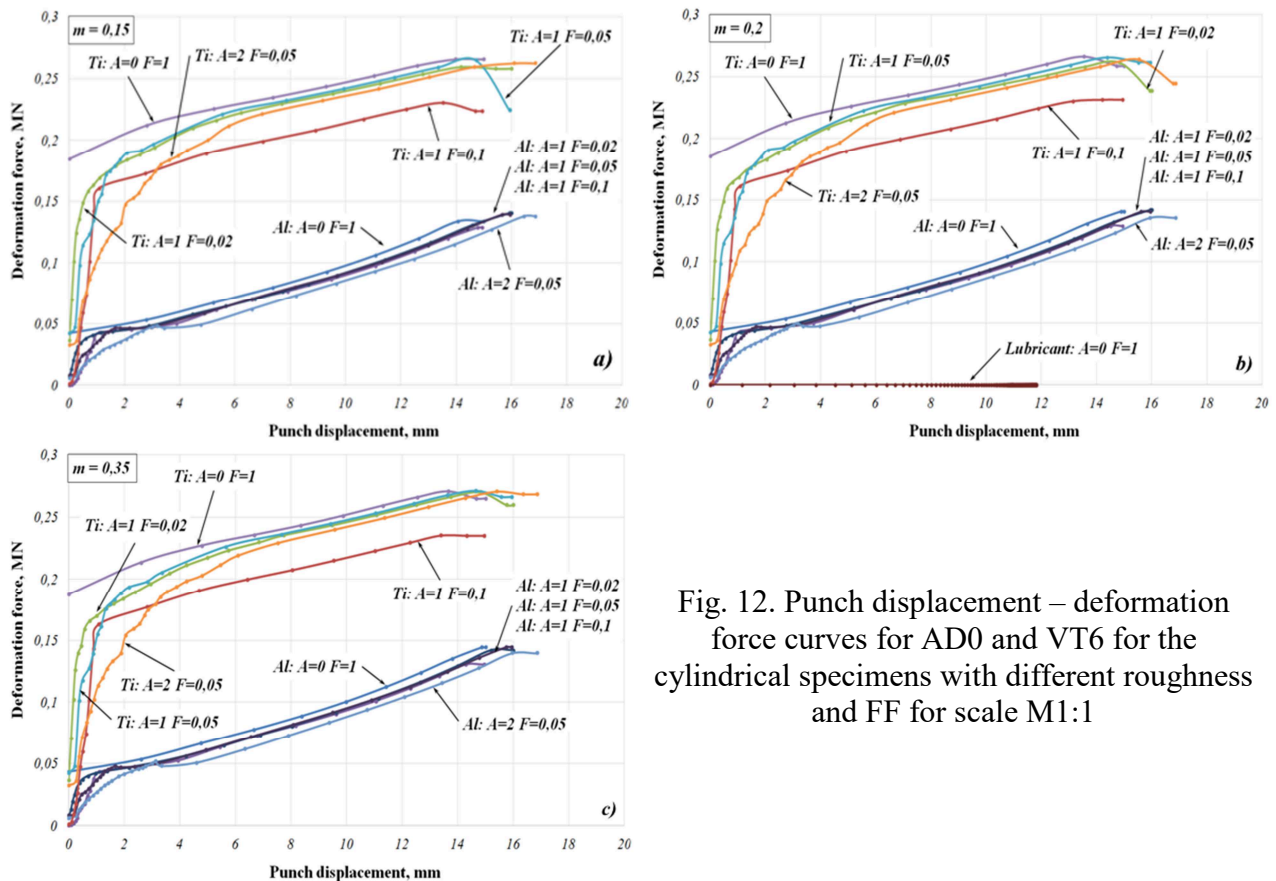


Fig. 12. Punch displacement – deformation force curves for AD0 and VT6 for the cylindrical specimens with different roughness and FF for scale M1:1

Simulation: roughness influence (in ODMFT). Further information to the acting deformation force values were collected by compression of the lubricant-like material. For the sample thickness of 2, 6 and 10 mm the maximal force values were equal to 150, 450 and 750 N correspondingly. With the increase of the peaks number of the inlay rough plate, the force growth was more relevant. All curves for the rough surfaces neared the curve for the sample with ideal surface (A0F1) to the point F1 (Fig. 2). At the same time, the curves for the rough surfaces lay upon the ideal case. These additional force amount was resulted due to non-uniform material flow in radial direction induced by local propagation resistance due to streamlining of the asperities (Fig. 14a –c) and (not investigated) resistance to propagation due to turbulence zone during fluid flow. In this sense, the material flow generates the wave. The wave propagates in the same direction with the velocity and exert pressure on the peaks. The highest tangential stresses located on the top of the asperities allocated at the beginning of the wave. For small asperities, the tangential stresses could overcome their yield stress value that will result their deformation or failure. The middle stresses changes from zero in the free flow area up to 1,2 MPa. The field of the middle stresses changes more intensive in radial direction as in vertical directions that underline the intensive material flow in radial direction.

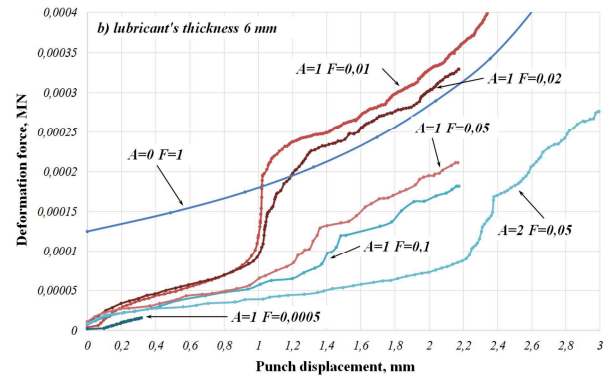
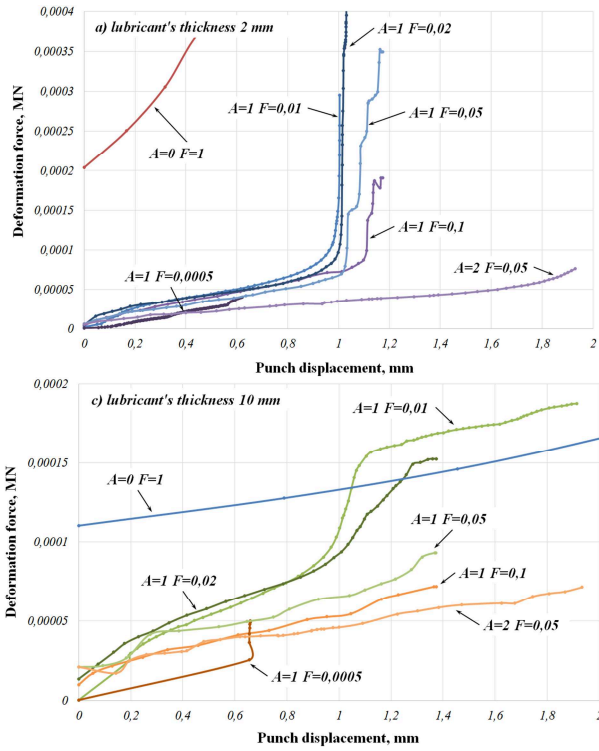


Fig. 13. Comparison of the force-displacement dependencies obtained in ODMFT for different A and F values (M1:1)

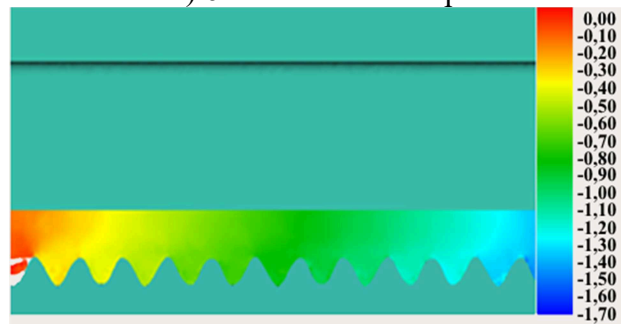
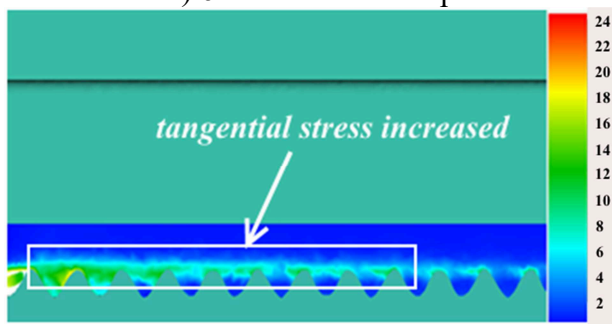
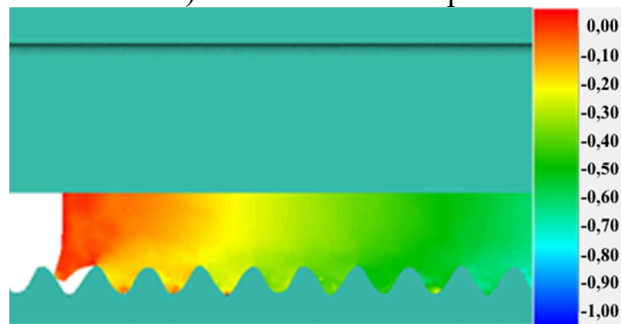
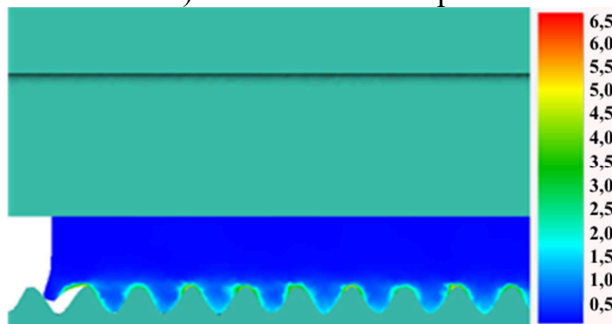
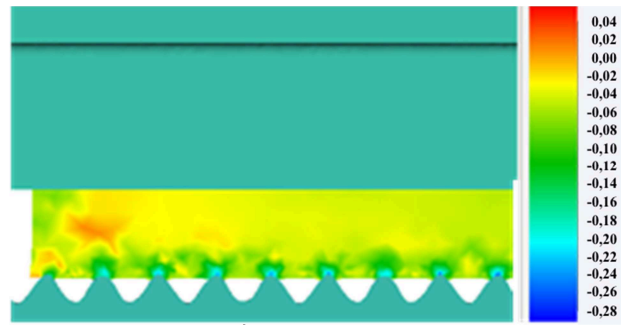
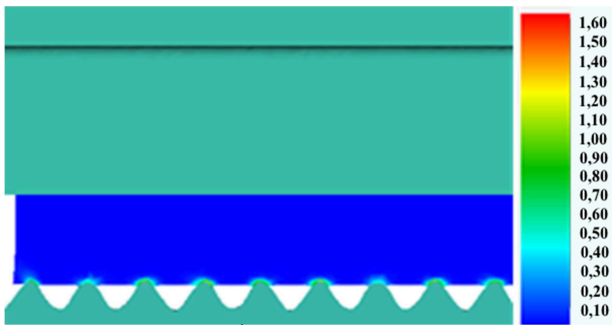


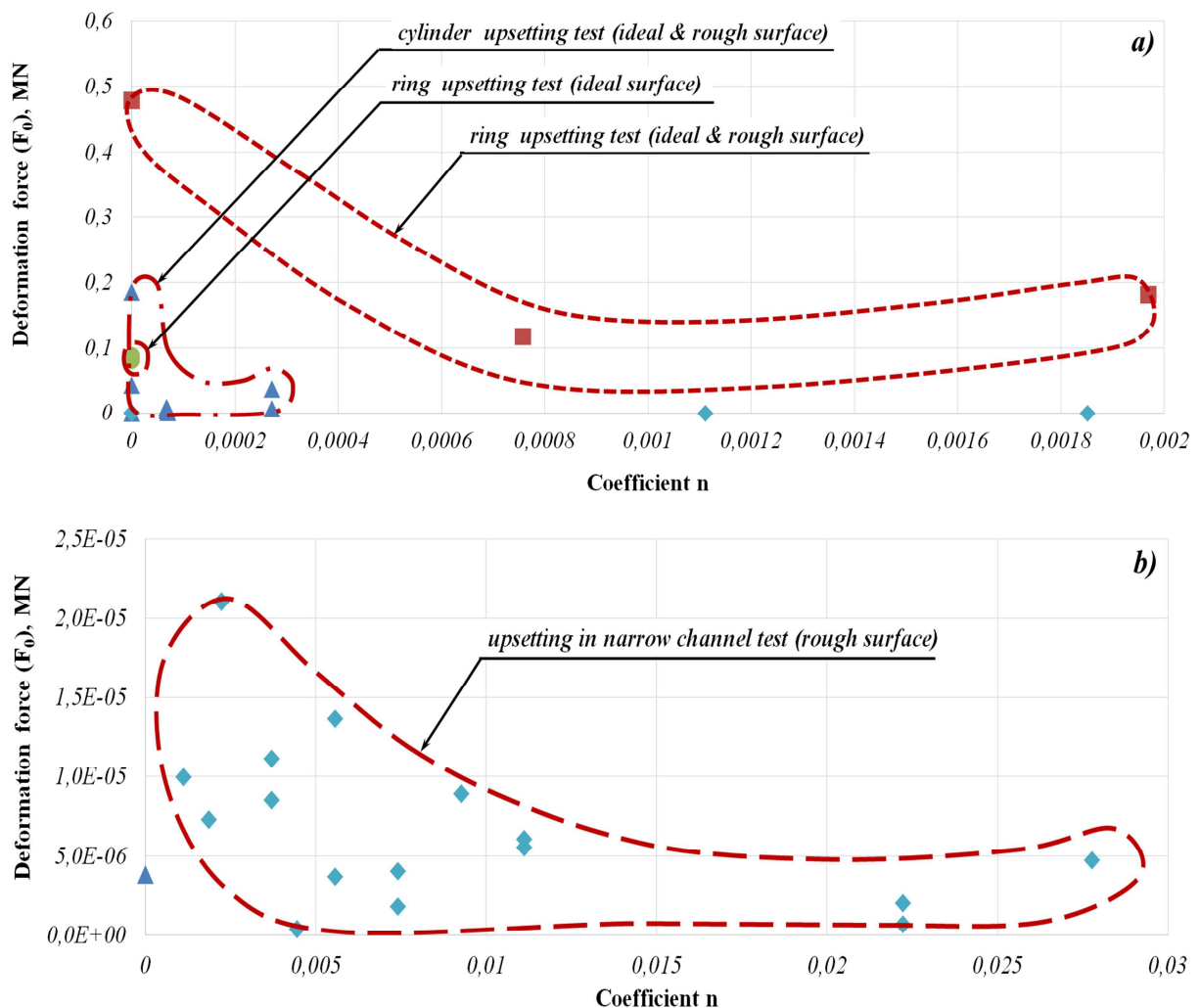
Fig. 14. Plastic deformation (a – c) and middle stresses in [MPa] (d – f) for A1F0,01 at initial lubricant thickness of 6 mm

Experiment: RCT. The friction coefficient was determined based on the nomograms obtained experimentally elsewhere [31]. It was equal to 0,24 for turning surface and 0,3 for grinding surface. The evaporation of the base of the lubricant was achieved and no hydrodynamic effects occurred. As it was expected, for the dry friction conditions the friction coefficient increased with increasing the area surface contact, i.e. the rougher the surface is, the higher is the friction coefficient. From this point of view the results correlates well with the primary understanding the reason of the force grow (Fig. 2).

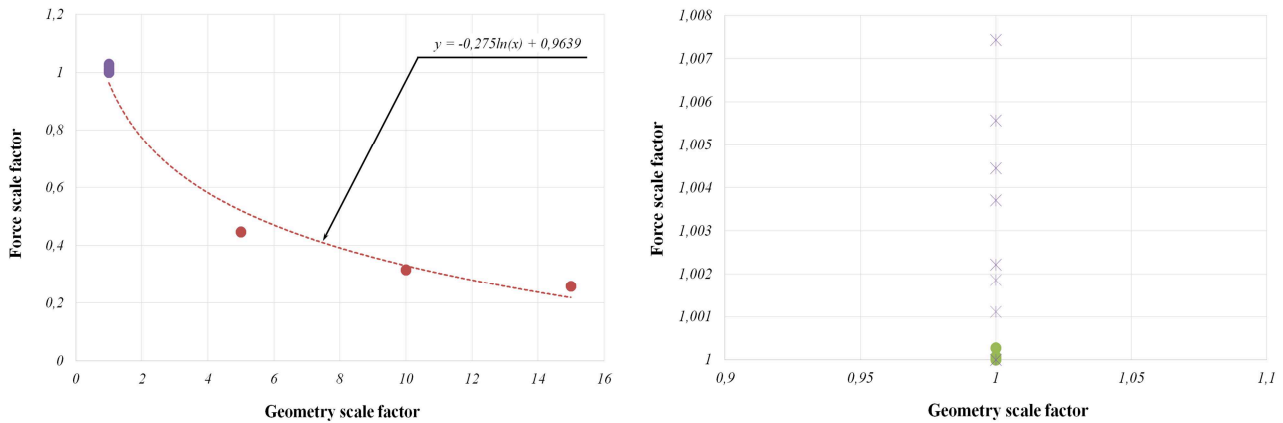
General validation. Representing the results as a function in coordinates of number of peaks, the punch surface contacts at first with, against the deformation force give uncertainties, i.e. both the surfaces with and without asperities in several cases provided the same force values. In fact, the deformation force applied not pointwise or linearly but distributed on the area and in the volume. That is why the amount of peaks is better to relate to the surface or volume (Fig. 15-I). The calculation of coefficient n was done in accordance with the Eq. 7 and the graphical representation is given in the Fig. 15-Ia. The enlarged area (Fig. 15-Ib) entrapped the values corresponded the ODMFT. For ideal surfaces (A0F1) the data points lay on the ordinate axis. The more n is, the more force is needed (for the same volume), but depends on the volume the tendency is reversible.

$$n = \frac{N}{V}, \quad (7)$$

where N – the amount of peaks; V – workpiece volume, [mm³].



I) roughness-to-volume coefficient against deformation force cloud of points for the RCT, CUT and ODMFT for common area (a) and for unique area (b)



II) scale function for the RCT, CUT and ODMFT for common (left) and for unique area (right)

Fig. 15. General validation results

Further the presented elsewhere [32] coupling equation for force and geometry scale factors could be extended by Eq. 7 and presented in the following form:

$$\lambda_F = \frac{e^n}{\sqrt{\lambda_G}}, \quad (8)$$

where λ_F – force scale factor; λ_G – geometry scale factor.

The graphical representation of the Eq. 8 is given in the Fig. 15-II. For calculated points the correspondent approximation logarithmic curve can be pointed out. The small region between 1 and 1,005 (the unique area) represent the concentration of points that correspond the ideal surfaces (A0F1) and scales M1:1.

Conclusions and outlooks

In the part of the numerical simulation of geometry distortion of the samples without roughness (Fig. 8a, b), a light disturbance can be obtained additionally at the samples with artificial roughness. Comparing the force – displacement reference curves (Fig. 8d) with the correspondent curves for rough samples (Fig. 12) obtained in CUT the same form is good recognized. Within the first steps before the rough surface will turn into the flat one due to remeshing procedure the curves from the Fig. 12 swung near the reference line presented in the Fig. 8d. In this case, we can draw the line with the real continuous stepwise asperities' breaking, where the force values drop down and grow up.

Lubricant's compression in RCT (Fig. 10d) and CUT (Fig. 12b) resulted small forces, whereby the ratio of the forces to perform the deformation of the solid and the liquid phases restricted to 100. Taking into account the real sizes of the asperities (μm -range (10^{-6} m) for real microroughness and mm-range (10^{-3} m) for simulated artificial roughness), the expected deformation force will be approximately reduced up to 10^5 times in comparison to the necessary deformation force of the sample volume, i.e. 10^2 multiplied with 10^3 . Such wide geometry ranges did not allow to perform the simultaneously computation for macro- and micro-force-deformation characteristics orderly.

The asperities (peaks) subjected to damage continuously either by the axial compression (punch) or tangential (lubricant flow) forces. Simultaneously the higher the force gradient is, the higher the risk of turbulent lubricant flow and higher surface friction prevented the continuous flow of the solid phase (Fig. 14).

The found influence of the artificial roughness on the force characteristics depends on the geometric sizes (Eq. 8) can be fitted by the natural logarithmic function good enough (Fig. 15-II). Further, the Eq. 8 should be extended through coupling with the real roughness or surface

topography terms. Also probably, another mathematical interpretation between the geometry and force characteristics have to be declared for microlevel and/or nanolevel.

As it was expected, the standard understanding of the geometry changes depends on the friction intensity had been computed quite realistic. In addition, the key role of scaling factor was represented. The influence of the friction factor and roughness on the deformation force for CUT is evident but more implicit for this study.

References

- [1] A.N. Petrov, B.A. Loginov, M.A. Petrov, Blank productions in mechanical engineering 4 (2016) 42-46 (*in Russian*).
- [2] G.T. Smith, Industrial Metrology: surfaces and roundness, Springer-Verlag, London, 2002.
- [3] G. Kerckhofs, G. Pyka, M. Moesen, S.V. Bael, J. Schrooten, M. Wevers, High-resolution micro-CT as a tool for 3D surface roughness measurement of 3D additive manufactured porous structures, *Adv. Eng. Mater.* 15(3) (2013) 153-158.
- [4] P. Petrov, J. Bast, M. Petrov, V. Voronkov, M. Schajchulov, Numerische Vergleichsanalyse der Methoden zur Abschätzung der Reibung in Umformprozessen, *Tribol. Schmierungstech.* 5 (2011) 10-14 (*in German*).
- [5] M. Petrov, P. Petrov, R. Yafaev, To the Question on the Friction Assessment Methods Applied for Metal Forming Operations, *Key Eng. Mat.* 651-653 (2015) 522-529.
- [6] E. Rabinowicz, Friction and Wear of Materials, second ed., Wiley, New York, 1995.
- [7] A.V. Chichinadze, Fundamentals tribology, Mashinostroenie, Moscow, 2001(*in Russian*).
- [8] Y.-R. Jeng, Experimental study of the effects of surface roughness on friction, *Tribol. T.* 3(3) (1990) 402-410.
- [9] E. Doege, B. Laackman, B. Kischnick, Fractal geometry used for the characterisation of sheet surfaces, *Annal. CIRP* 44(1) (1995) 197-200.
- [10] T. Hisakado, Surface roughness and deformation of contact asperities between a rough and a flat surface, *Wear* 35(1) (1975) 53-61.
- [11] T. Hisakado, Effect of surface roughness on contact between solid surfaces, *Wear* 28(2) (1974) 217-234.
- [12] M.P.F. Sutcliffe, Surface asperity deformation in metal forming processes, *Int. J. Mech. Sci.* 30(11) (1988) 847-868.
- [13] J. Stahlmann, E.R. Nicodemus, S.C. Sharma, Surface Roughness Evolution in FEA Simulations of Bulk Metal Forming Process, *Wear* 288 (2012) 78-87.
- [14] D. Leu, Modeling of Surface Roughness Effect on Dry Contact Friction in Metal Forming, *Int. J. Adv. Manuf. Tech.* 57(5-8) (2011) 575-584.
- [15] P. L. Menezes, Kishore, S. V. Kailas, Influence of Surface Texture and Roughness Parameters on Friction and Transfer Layer Formation during Sliding of Aluminium Pin on Steel Plate, *Wear* 267(9-10) (2009) 1534-1549.
- [16] P. Groche, J. Stahlmann, J. Hartel, M. Koehler, Hydrodynamic effects of macroscopic deterministic surface structures in cold forging processes, *Tribol. Int.* 42 (2009) 1173-1179.
- [17] P. Groche, C. Mueller, A. Jahn, Effects of the Tool Lubrication in Cold Forging, *Tribol. Lett.* 53 (2014) 599-605.

- [18] P. Groche, P. Kramer, S. Zang, V. Rezanov, Prediction of the Evolution of the Surface Roughness in Dependence of the Lubrication System for Cold Forming Processes, *Tribol. Lett.* 59 (2015) 1-9.
- [19] L.-F. Chiang, H. Hosokawa, J.-Y. Wang, T. Uesugi, Y. Takigawa, K. Higashi, Investigation on Dynamic Friction Properties of Extruded AZ31 Magnesium Alloy Using by Ring Upsetting Method, *Mater. Trans.* 51(7) (2010) 1249-1254.
- [20] K.H. Jung, H.C. Lee, J.S. Ajiboye, Y.T. Im, Characterization of Frictional Behaviour in Cold Forging, *Tribol. Lett.* 37 (2010) 353-359.
- [21] C. Hubert, N. Bay, P. Christiansen, R. Deltombe, L. Dubar, M. Dubar, A. Dubois, Analysis of fluid lubrication mechanisms in metal forming at mesoscopic scale, *Annal. CIRP* 61(1) (2012) 271-274
- [22] Y. Carretta, N. Legrand, M. Laugier, J.-P. Ponthot, Numerical Simulations of Asperity Crushing – Application to cold rolling, *AIP Conf. Proc.* 1353 (2011) 1770-1775
- [23] Yu.A. Karpenko, A. Akay, A numerical model of friction between rough surfaces, *Tribol. Int.* 34 (2001) 531-545.
- [24] R.S. Eriksen, S. Weidel, H.N. Hansen, Tribological influence of tool surface roughness within microforming, *Int. J. Mater. Form.* 3(Suppl. 1) (2010) 419-422.
- [25] N. Biba, S. Stebunov, A. Vlasov, Material forming simulation environment based on QForm3D software system, information on http://www.qform3d.ru/files_ru/2008_0001_0.pdf (*stand on the 15.05.2016*).
- [26] A.N. Levanov, V.L. Kolmogorov, S.P. Burkin, B.R. Kartak, Yu.V. Ashpur, Yu.I. Spasskiy, Contact friction in metal forming processes, *Mashinostroenie, Moscow, 1975 (in Russian)*.
- [27] P.A. Petrov, V.I. Perfilov, M.A. Petrov, Experimental and numerical investigation of friction in hot isothermal deformation of aluminium alloy A92618, *Proceedings of the 7th International Esaform Conference on Material Forming*, ed. S. Storen, 2004, Trondheim, Norway
- [28] P. Petrov, M. Petrov, E. Vasileva, A. Dubinchin, Research on Friction during Hot Deformation of Al-Alloys at High Strain Rate, *Int. J. Mater. Form.* 1(Suppl. 1) (2008) 1255-1258.
- [29] D.V. Laptev, Yu. G. Kalpin, A.N. Petrov, The application of water-based lubricants with colloidal graphite for hot forging, *Proceeding of the conference on synthetic lubricants*, ed. András Zakar, 12-14 September 1989, Sopron, Hungary
- [30] A. Petrov, P. Petrov, M. Petrov, Research into water-based colloidal-graphite lubricants for forging of carbon steels and Ni-based alloys, *Int. J. Mater. Form.* 3(Suppl. 1) (2010) 311-314.
- [31] A.N. Petrov, Estimation of the friction coefficient by ring compression test subjected to hot deformation, *Izvestiya «MSTU «MAMI»* 1(1) (2012) 196-200 (*in Russian*).
- [32] M. Petrov, V. Voronkov, P. Petrov, D. Grishin, Numerical investigation of the hot isothermal process and force size-effect of a clutch-half forming, *Key Eng. Mat.* 611-612(2014) 1608-1616.